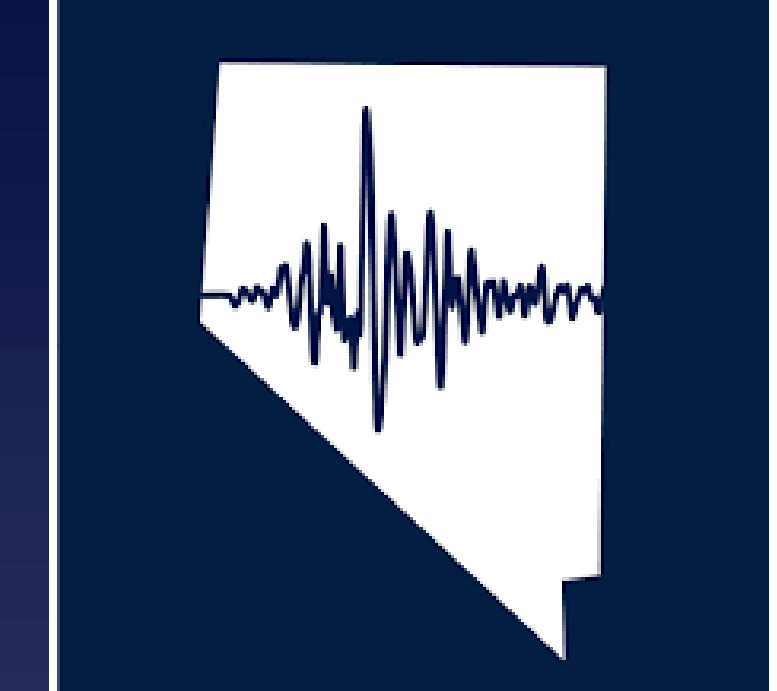


SOLVING THE NEAR-FAULT DATA SCARCITY PROBLEM FOR NORMAL-FAULTING EARTHQUAKES USING DYNAMIC RUPTURE SIMULATIONS



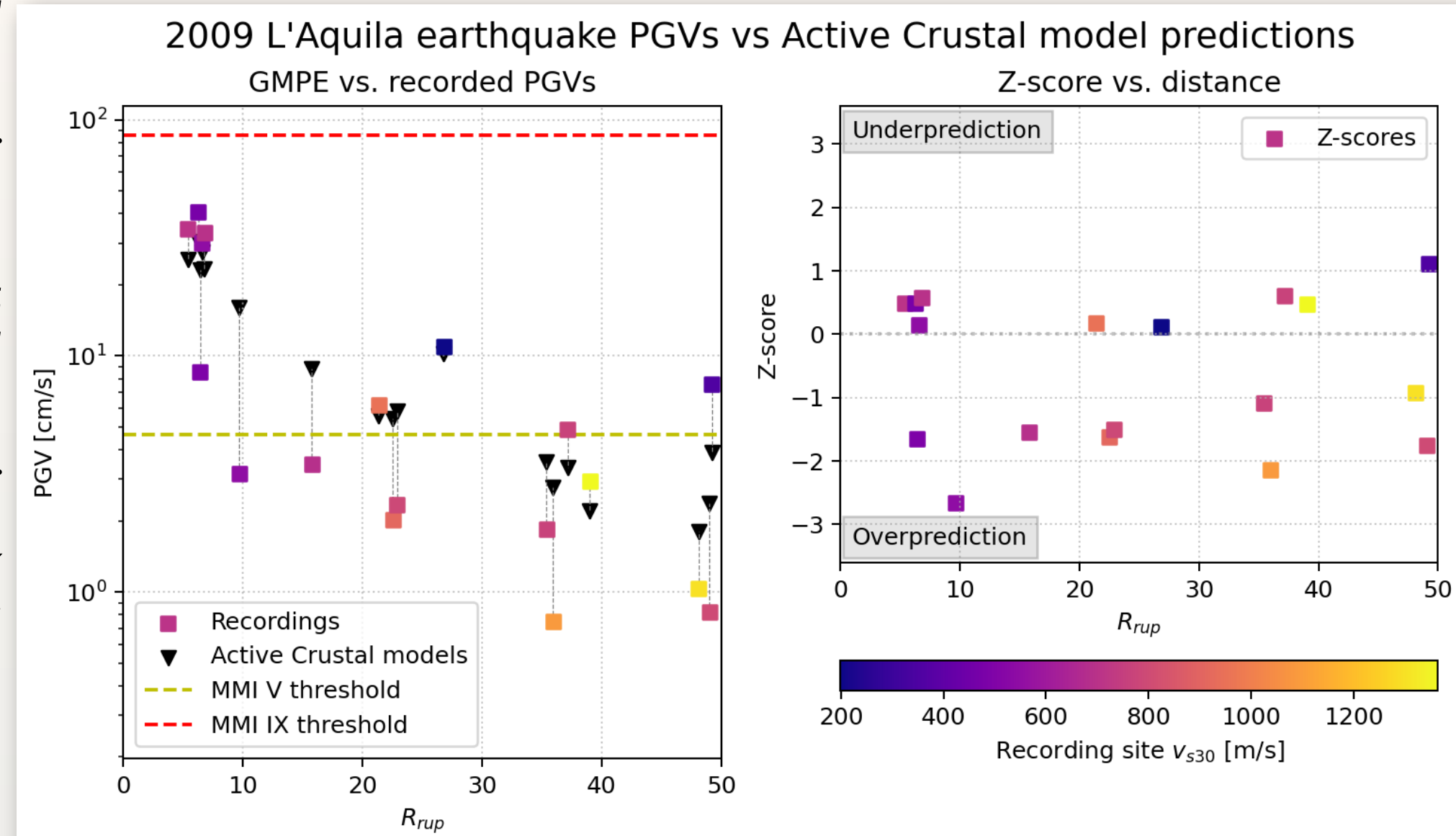
YAIR FRANCO, DANIEL TRUGMAN
NEVADA SEISMOLOGICAL LABORATORY, UNIVERSITY OF NEVADA, RENO

ABSTRACT #1875689
AGU 2025

BACKGROUND

- Normal faults under populated areas are known to have high damage potential
 - 2009 L'Aquila, 2016 Amatrice and Norcia earthquakes
- Basin and Range seismicity dominated by normal faulting earthquakes
 - Scarce record due to sparse instrumentation at the time of largest normal-slip events (1915, 1954)
- 2023 U.S. National Seismic Hazard Model (NSHM) active crustal models derived from scarce normal-slip strong motion data
 - ASK14 dip-slip fault hanging wall term generalized from kinematic simulations of thrust faults (1)
- Data scarcity may cause mischaracterization of seismic hazard in populations close to normal faults (e.g. see Figure 1), including cities like Reno, Salt Lake City, etc.

Figure 1: Comparison of recorded PGVs and GM predictions for the M6.3 2009 L'Aquila earthquake. Models use station-specific distance and site parameters. Left plot shows GMDB (2) vs. predicted PGVs. Right plot shows z-scores. Data plotted against R_{rup} (distance from rupture plane). Stations color coded by V_{S30} . Modified Mercalli Intensity (MMI) thresholds for intensities V and IX are plotted as yellow and red dotted lines, respectively.



METHODS

- Run a suite of dynamic rupture simulations in SeisSol
- Normal and reverse-slip simulations based on TPV10 benchmark test (3)
 - Fault dimensions: 30x15 km
 - Dip: 60° (variable)
 - Nucleation patch: 3x3 km
 - Hypocenter: 12 km down-dip from midpoint of surface fault trace
 - Fault ruptures the surface
 - Embedded in 100x100x42-km domain
 - Depth-dependent stress parameters

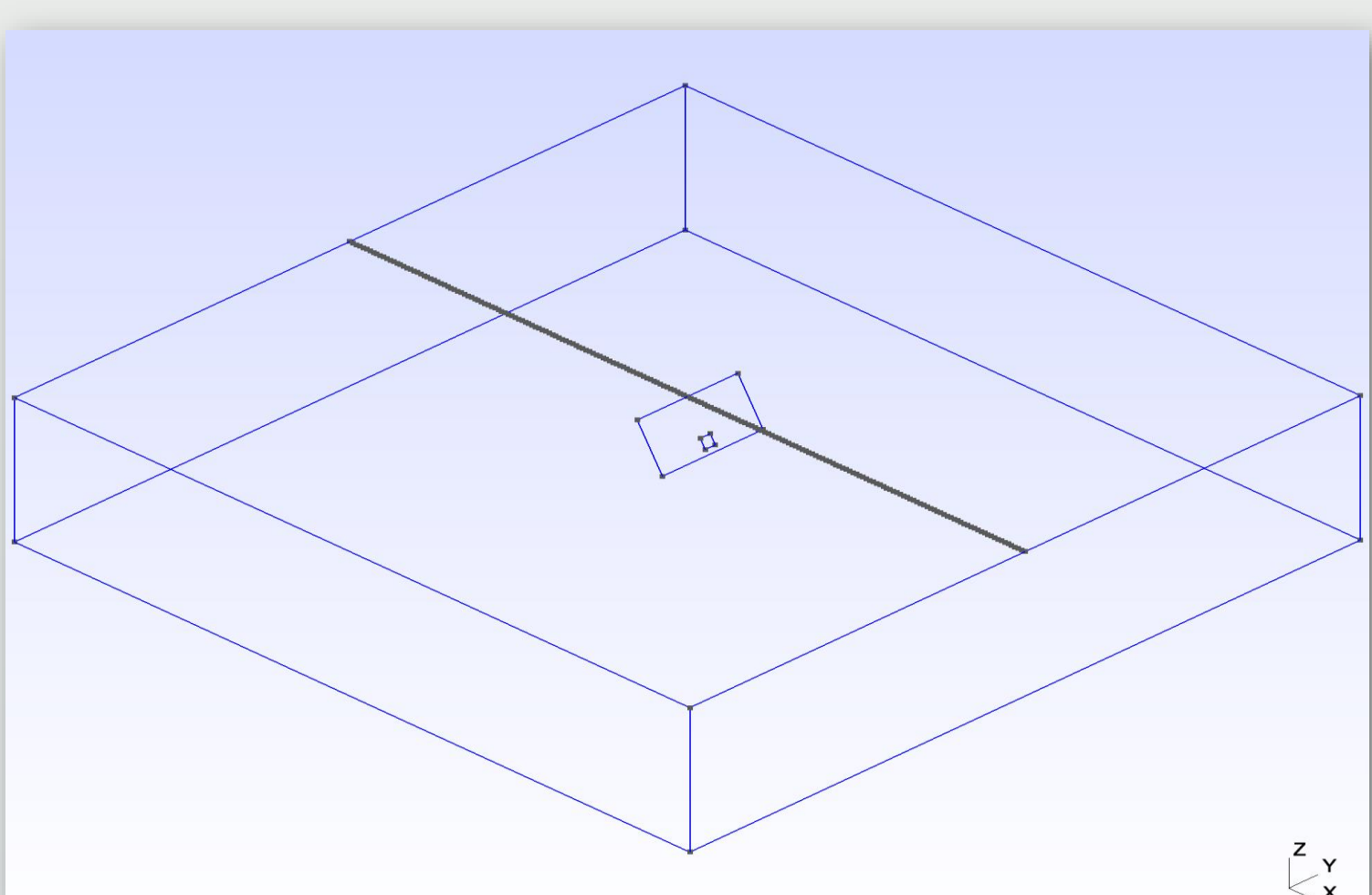
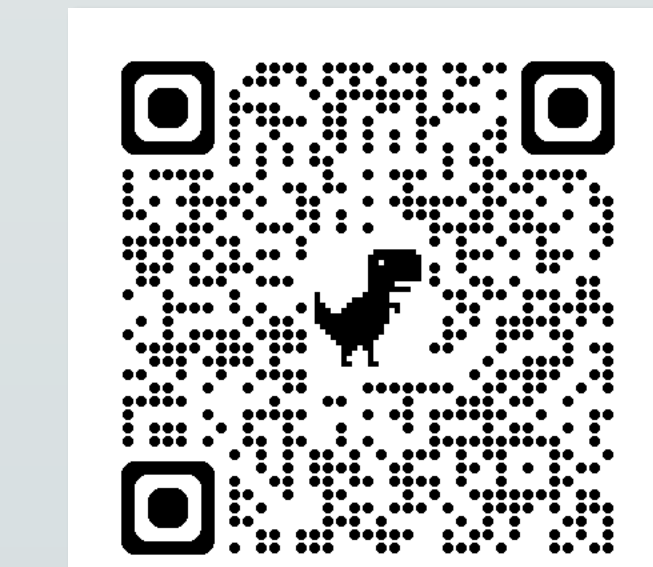


Figure 2: Example of 3D mesh used as SeisSol input for simulations. This is the case of a 60°-dipping fault in a 100x100x42-km domain. Also shown is the line along which PGV is calculated for GMPE comparisons. This line is perpendicular to the surface fault trace and crosses its midpoint.

- Variables:
 - Dip: 25-75° (5° increment) for both mechanisms
- Compare dynamic rupture simulation data to ground motion models
 - SeisSol data read from mesh output
 - RotD50 velocities computed from V_x and V_y data
 - Ground motion prediction data obtained via OpenQuake library (4)
 - Average of four Active Crustal models used in 2023 NSHM:
 - Boore et al., 2014 (BSSA14)
 - Abrahamson et al., 2014 (ASK14)
 - Campbell & Bozorgnia, 2014 (CB14)
 - Chiou & Youngs, 2014 (CY14)

Scan this QR code to view a digital version of this poster and supplemental materials like simulation animations. Alternatively, visit yairfranco.com/agu2025



RESULTS

- Base case (60° dip) SeisSol simulations return distribution patterns consistent with previous literature (5)
 - Stronger ground motions on hanging wall ($R_x > 0$) side
- Observed discrepancies:
 - Simulation returns ground motions lower than 1σ (standard deviation) below the GMPE median values
 - Dip angle in normal slip has strong effects on ground motion distributions not encapsulated by GMPEs
- GMPE vs. simulation data discrepancy increases with more extreme high/low-angle faulting
 - Near-fault ($R_x < 10$ km) PGVs over 1σ off from GMPEs in several cases
 - Strongest PGVs migrate to hanging wall ($R_x < 0$) in low-angle faulting cases, not seen in GMPEs
 - Reverse-slip PGVs significantly higher on footwall side than in normal-slip
 - Supershear rupture simulations (not shown here) return even stronger ground motions on hanging wall side

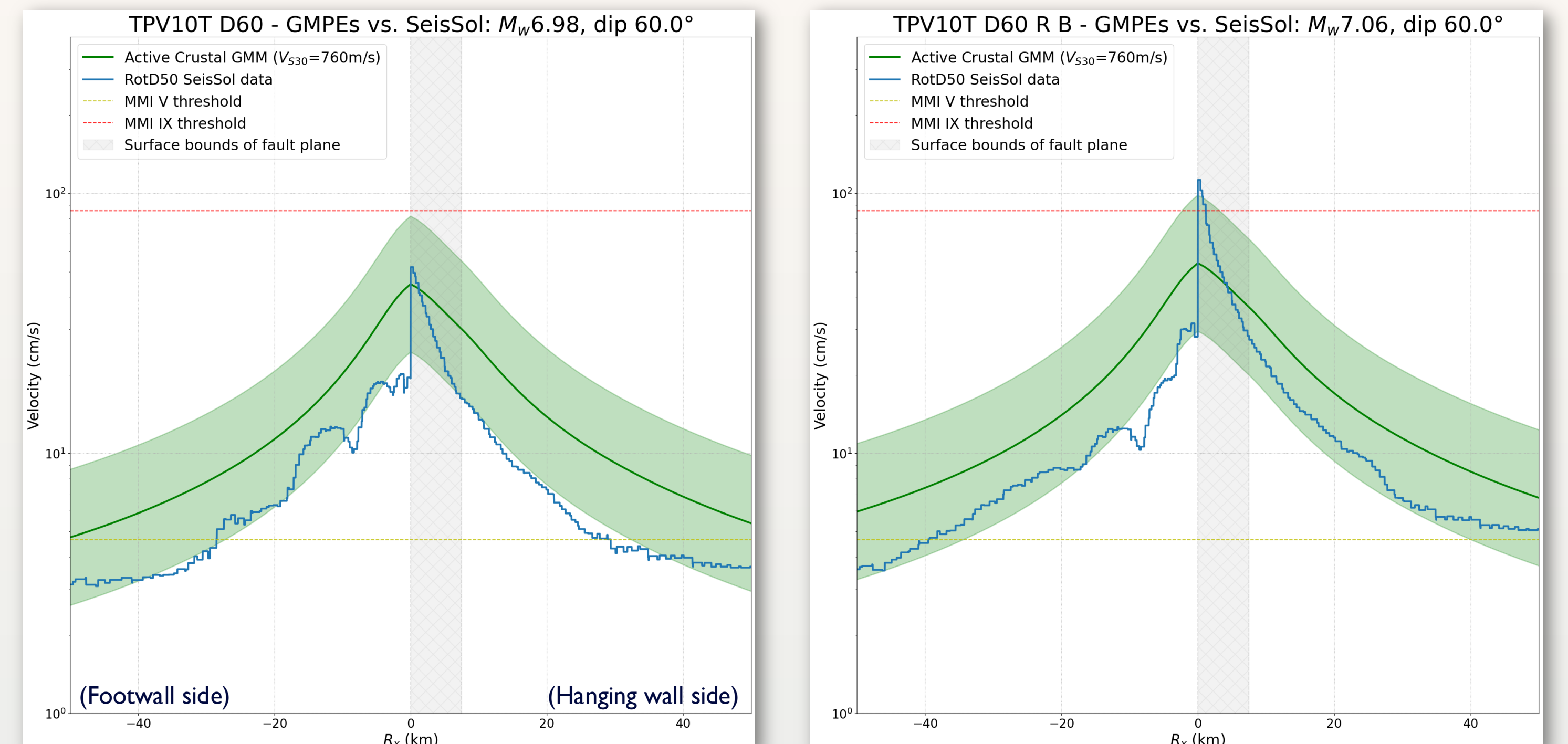


Figure 3: Results from a SeisSol simulation based on TPV10 (60°-dipping, 30x15 km fault rupturing the surface). RotD50 (rotation-independent median of horizontal motion) peak ground velocities (PGVs) computed from SeisSol data are plotted in log-y scale as a blue line. The average of the log-median of the four GMPEs previously listed, matching SeisSol rupture parameters, is plotted in log-y scale as a green line. Infill shows one log-standard deviation (1σ).

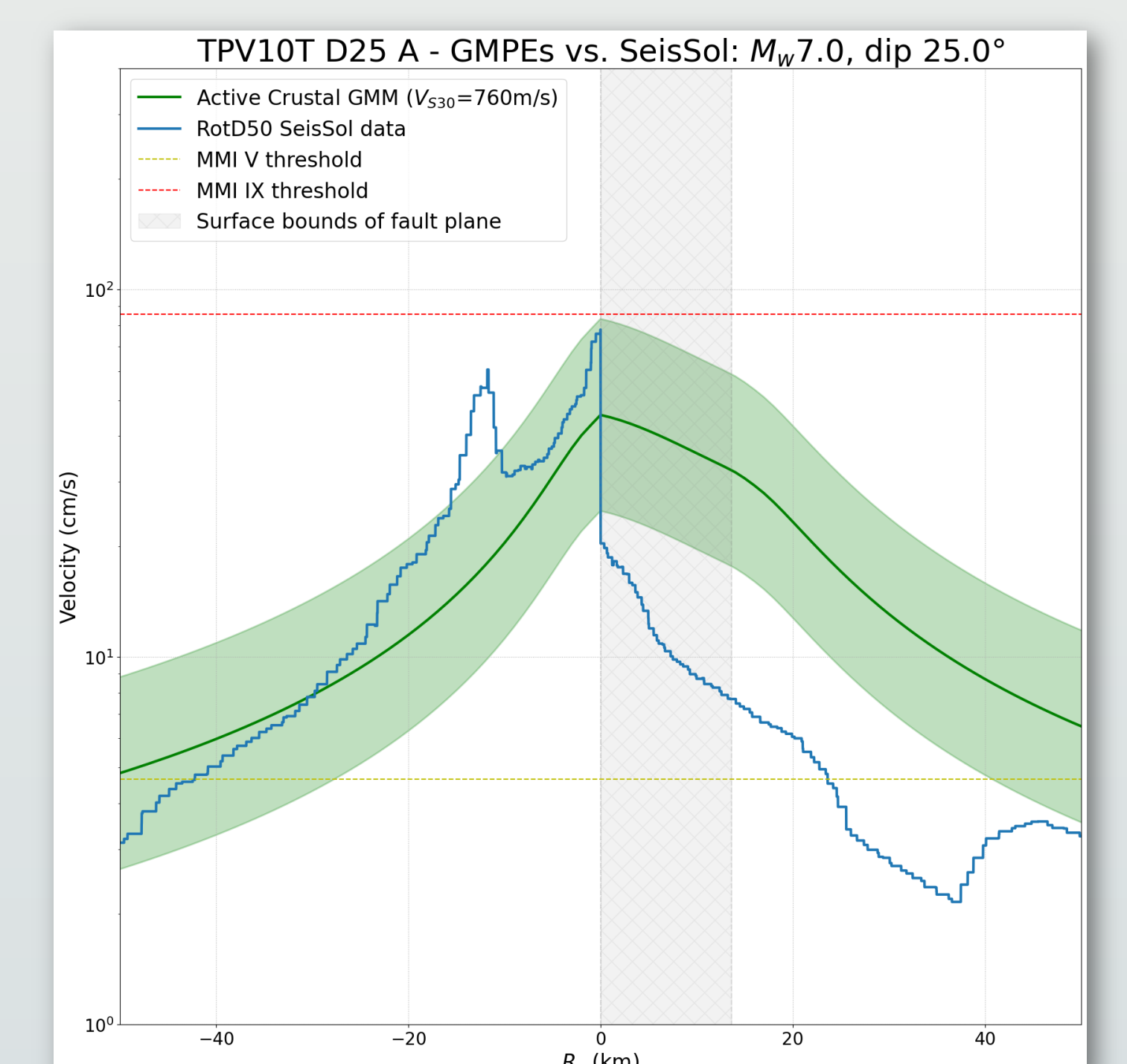
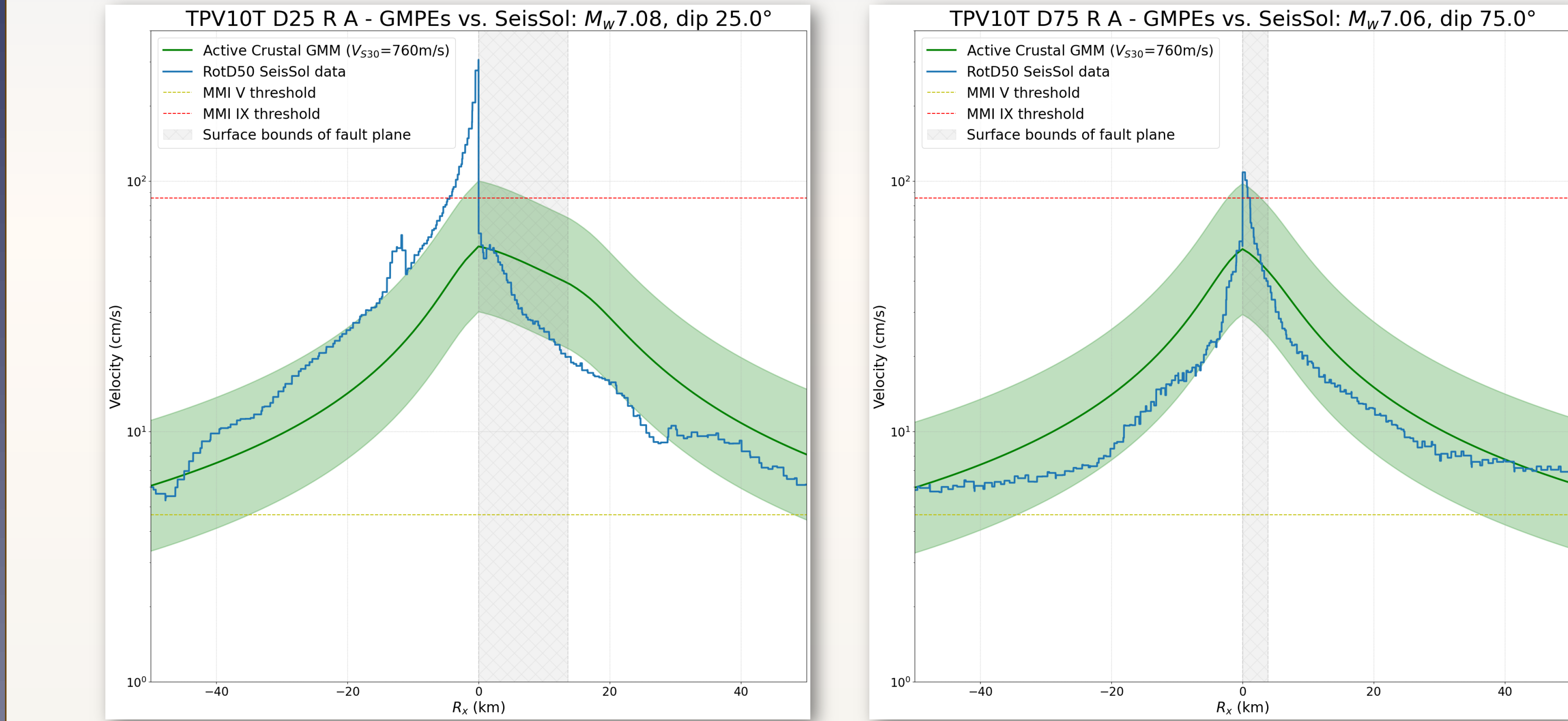
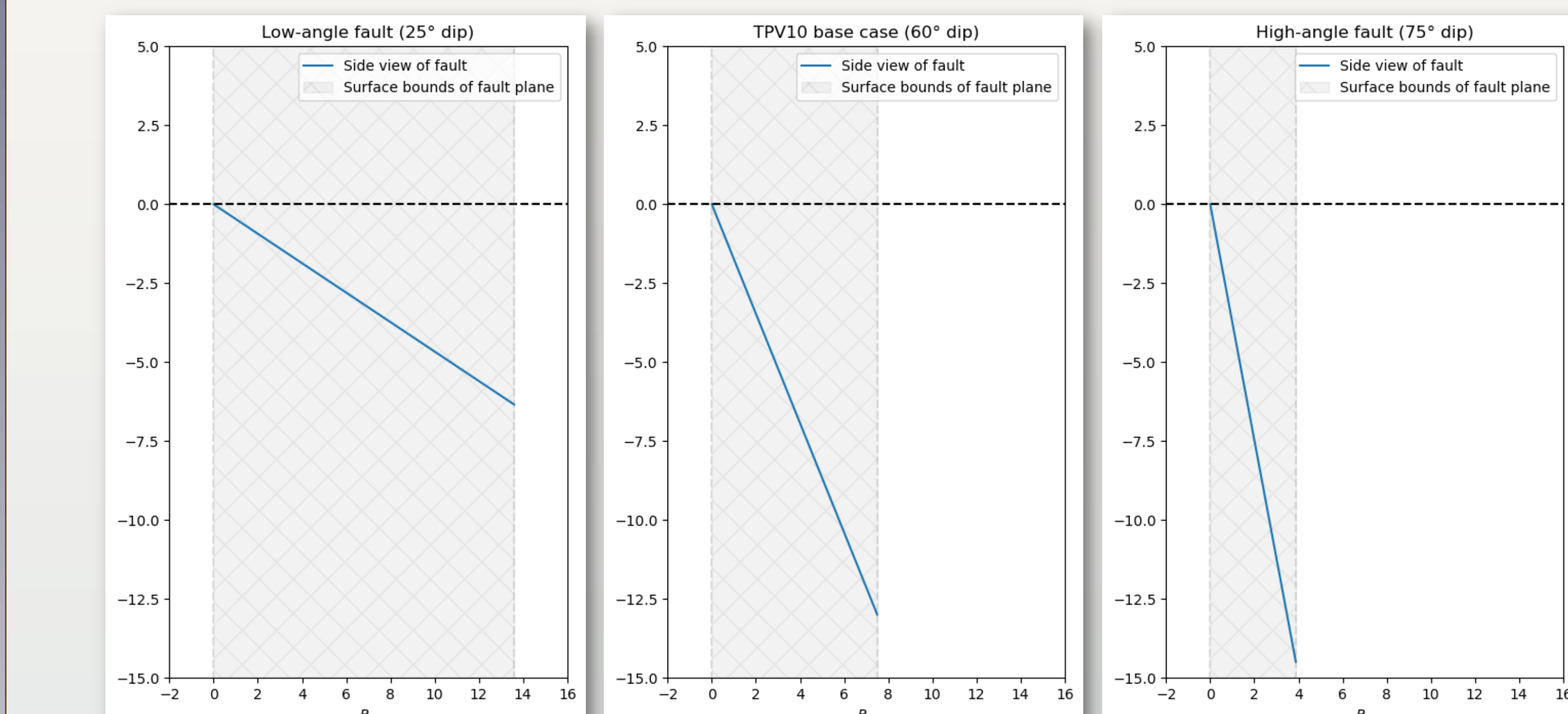


Figure 4: Same as Figure 2, but with data from a reverse-slip simulation. The only difference between these simulations is the down-dip fault traction, which has been reoriented to be up-dip. GMPEs rerun accordingly.



Figures 6a and 6b: SeisSol vs. GMPE data plotted as in 4a and 4b, but for reverse faulting. Note the difference in simulated PGVs between reverse and normal-slip earthquakes.



Figures 7a, 7b, and 7c: Dimensional references for (a) low-angle, (b) base case, and (c) high-angle faulting as shown in previous figures. Axes dimensions are identical for all three plots.

SUMMARY & FUTURE STEPS

- Normal and reverse-slip simulations have starkly different peak PGVs and ground motion distributions
 - Simulated ground motion for dip-slip earthquakes should be distinguished by direction (normal/reverse) when used as substitute for real data
- 2023 NSHM in Basin and Range, if purely based on GM predictions, may mischaracterize hazard
- Future GMPEs would benefit from richer near-fault strong motion data, while dynamic rupture simulations can temporarily substitute for scarce data in current models
- Future work will encompass tests applying basin topography and ground velocity variations and possible earthquake scenarios

REFERENCES

- Donahue & Abrahamson. "Simulation Based Hanging Wall Effects." *Earthquake Spectra*, 2014.
- Buckkreis et al. "Archive of an Earthquake Ground Motion Relational Database (GMDB) for Engineering Applications." *DesignSafe-CI*, 2025.
- Harris et al. "A Suite of Exercises for Verifying Dynamic Earthquake Rupture Codes." *Seismological Research Letters*, 2018.
- Pagan et al. "OpenQuake Engine: An Open Hazard (and Risk) Software for the Global Earthquake Model." *Seismological Research Letters*, 2014.
- O'Connell et al. "Influence of Dip and Velocity Heterogeneity on Reverse- and Normal-Faulting Rupture Dynamics and Near-Fault Ground Motions" *Bulletin of the Seism. Soc. Of America*, 2007.

ACKNOWLEDGEMENTS

This work was supported by National Science Foundation Awards RISE-2531037 and EAR-2121666, NASA Award 80NSSC24K0736, and the Nevada Division of Emergency Management Award HMGP DR-4523-08-BP.